THE JOURNAL OF PHYSICAL CHEMISTRY B

Article

pubs.acs.org/JPCB

Limited Perturbation of a DPPC Bilayer by Fluorescent Lipid Probes: A Molecular Dynamics Study

David G. Ackerman,[†] Frederick A. Heberle,[‡] and Gerald W. Feigenson*[,†]

[†]Department of Molecular Biology and Genetics, Cornell University, Ithaca, New York 14853, United States

[‡]Biology and Soft Matter Division, Neutron Sciences Directorate, Oak Ridge National Laboratory, Oak Ridge, Tennessee 37831-6100, United States

Supporting Information

ABSTRACT: The properties of lipid bilayer nanometer-scale domains could be crucial for understanding cell membranes. Fluorescent probes are often used to study bilayers, yet their effects on host lipids are not well understood. We used molecular dynamics simulations to investigate perturbations in a fluid DPPC bilayer upon incorporation of three indocarbocyanine probes: DiI-C18:0, DiI-C18:2, or DiI-C12:0. We find a 10−12% decrease in chain order for DPPC in the solvation shell nearest the probe but smaller effects in subsequent shells, indicating that the probes significantly alter only their local environment. We also observe order perturbations of lipids directly across from the probe in the opposite leaflet. Additionally, the DPPC headgroup phosphorus-to-nitrogen vector of lipids nearest the probe exhibits preferential orientation pointing away from the DiI. We show that, while DiI probes perturb their local environment, they do not strongly influence the average properties of "nanoscopic" domains containing a few hundred lipids.

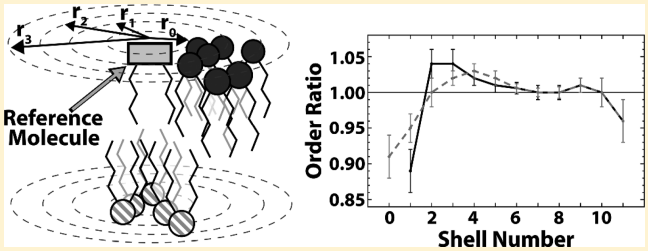

1. INTRODUCTION

Probe-based studies greatly aid our understanding of lipid membranes. Fluorescent probes in particular have proven useful, and bilayer properties studied with fluorescence techniques include order,[1] hydration and polarity,[2] electrostatic potential,[3] lipid lateral diffusion,[4] and phase state.[5] In recent years, fluorescence spectroscopy (reviewed in ref 6) and microscopy (reviewed in refs 7 and 8) have played an important role in elucidating the lateral organization of model membranes. Fluorescence studies continue to drive the membrane raft field, including recent observations of Ising-like critical behavior[9] and stable nanoscopic phase domains.[10]

Accurate fluorescence experiments, especially when concerning raft-sized domains, rely on the assumption that the probes do not alter the properties they are measuring. However, fluorescent probes report only on their local environment. Therefore, effects that are negligible in the bulk may still be significant in the smaller reporting region of the probe. For instance, the local dielectric field near the probe—such as that produced by the charge-dense lipid headgroups—can affect probe fluorescence, while lipid order near the probe can affect partitioning of the probes and (for spin-labeled probes) can also alter their order and motion. If the probes themselves affect the headgroup orientation or order of nearby lipids, they may be reporting on altered environments.

Clearly, probe-induced perturbations must be assessed independently from the information reported by the probe, and several techniques have proven useful in this regard. In bilayers doped with fluorescent probes, differential scanning calorimetry[11] and ^{2}H NMR[12] have been used to detect changes in the bilayer gel/fluid transition temperature, X-ray diffraction has been employed to measure differences in average bilayer structure,[13] and ^{1}H NMR has been used to measure changes in motional freedom of the host lipid.[14] Each of these techniques reports on the average properties of a large number of lipids. Typically, significant perturbations are not detected until the probe concentration exceeds several mole percent, although exceptions are reported.[12] Bulk membrane properties are inherently insensitive to the very local perturbations induced by a probe at the dilute concentrations (<0.1 mol %) typically found in spectrophotometric experiments. Two different but related questions can be posed: To what extent does the probe report on a perturbed local environment? And, how far out from the probe is the lipid perturbed?

Molecular dynamics (MD) simulations can provide insight into bilayer structure and dynamics that might otherwise be impossible to obtain experimentally. Simulations offer a unique way of characterizing the spatial dependence of perturbations induced by a probe, including local changes. MD studies of bilayers containing fluorescent probes have appeared in the literature, aimed at understanding the location and dynamics of the fluorophore and the distance dependence of their perturbative effects within the bilayer.[15−18] Reviewing several of these studies, Loura and Ramalho emphasized the important

Received: January 9, 2013
Revised: April 1, 2013
Published: April 2, 2013

   dx.doi.org/10.1021/jp400289d | J. Phys. Chem. B 2013, 117, 4844−4852

distinction between first-shell lipids and the average properties of all lipids in the simulation.[19] In a recent MD study, the indocarbocyanine probe DiI-C18:0 was found to increase the *average* order and thickness of a fluid DPPC bilayer, while changing *average* headgroup orientation as measured by the phosphorus-to-nitrogen (P−N) vector.[20] Here, we used MD to examine the spatial dependence of such perturbations in a DPPC bilayer from three types of positively charged DiI: DiI-C18:0, DiI-C18:2, or DiI-C12:0.

We examined perturbations as a function of distance from the DiI molecules. This allowed us to analyze the length scale over which the dye perturbs its environment. We saw that, on a very small scale, the DiI molecules disorder their local environment and cause reorientation of the local lipid headgroups. However, these effects are short-range, and overall, the dye has a negligible effect on a patch of a few hundred lipids.

2. SIMULATION METHODS

All MD simulations were performed using version 4.5.3 of the Groningen Machine for Chemical Simulations (GROMACS),[21] using the ffg53a6 force field[22] with Berger lipid parameters.[23]

2.1. Simulation Setup. The molecular structures used in this study are shown in Figure 1. A DiI-C18:0 PDB file was

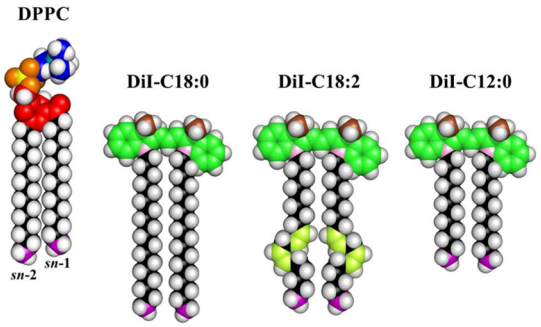

Figure 1. Molecular structures used in this study. DPPC: choline−$(CH_2)_2$ carbon (blue) and nitrogen (cyan), phosphate oxygen (orange) and phosphorus (yellow), glycerol−carbonyl (red), methylene carbon (black), terminal methyl (purple). DiI: chromophore (green), headgroup methyl (brown), nitrogen (pink), methylene carbon (black), alkene carbon (yellow-green), terminal methyl (purple). This color coding is used in Figures 3, 4, 5, and 10.

constructed using the PRODRG2 server (http://davapc1.bioch.dundee.ac.uk/prodrg/), and its topology file (including charge distribution) was obtained from ref 24, with some atom types changed to match the force field. DiI-C12:0 was constructed by truncating the DiI-C18:0 alkyl chains. Similarly, DiI-C18:2 was constructed by replacing the appropriate single bonds in the alkyl chains of DiI-C18:0 with *cis* double bonds, using parameters from the oleoyl chain of POPC (http://moose.bio.ucalgary.ca/index.php?page=Structures_and_Topologies).[23] Topology files for the DiI probes are included in the Supporting Information (section S1). DPPC topology parameters were from Chiu et al.[25]

A total of 12 bilayer simulations were performed for each probe (DiI-C18:0, DiI-C18:2, or DiI-C12:0). The starting configurations of each lipid were identical for all 12 simulations with the exception of the inserted molecule, which was randomly rotated about its long axis. To ensure statistical independence of the 12 simulations, different random seeds were used to generate different initial velocities. The bilayer initially contained 512 DPPC molecules, constructed from an equilibrated DPPC bilayer with 128 total lipids (http://people.ucalgary.ca/~tieleman/download.html).[26] One DPPC molecule from each leaflet was then removed to provide space for insertion of a probe molecule. To minimize unfavorable interactions, all inserted molecules were initially placed so that they were slightly protruding out of the bilayer. As a control, we also performed 12 simulations in which a DPPC molecule (rather than a probe) was reinserted to ensure that the insertion step did not itself cause perturbations. Additional information regarding the simulation setup is included in the Supporting Information (section S2).

2.2. Simulation Conditions. After bilayer assembly, the systems were solvated using the simple point charge (SPC) water model,[26] with ∼29 waters per lipid. For the DiI-containing simulations, two chloride ions were added to cancel the net charge of the system. A 3 ns NVT temperature equilibration was performed at 323 K (i.e., fluid-phase DPPC) using the V-rescale thermostat with a time constant of 0.1 ps. During this time, the inserted molecules were pulled into the bilayer. A 60 ns production run was then performed in the NPT ensemble at 323 K and 1 atm, using the Nosé−Hoover thermostat and Parrinello−Rahman semi-isotropic barostat with 0.5 and 2 ps time constants, respectively. The first 10 ns of these runs were considered as additional equilibration, and only the final 50 ns were analyzed. Data for the production run were saved every 10 ps.

Periodic boundary conditions were applied in all three spatial directions, with x and y corresponding to the bilayer plane and z to the bilayer normal. Bond lengths were constrained using the LINCS algorithm,[27,28] and the particle-mesh Ewald (PME) method[29,30] was used for electrostatic interactions, with cubic interpolation order 4 and a Fourier transform grid spacing of 0.16 nm. A neighbor-list cutoff of 1.1 nm, short-range interaction cutoff of 1.1 nm, and Lennard-Jones interaction cutoff of 1.1 nm were also applied. The equations of motion were integrated *via* the leapfrog algorithm with a time step of 2 fs.[27,28]

2.3. Data Analysis Methodology: Shell Partitioning Scheme. Our primary objective is to understand the magnitude and spatial extent of probe perturbations, and to this end, we examined average properties of the host lipid (fluid phase DPPC) as a function of distance from the probe molecule. Following the procedure of Kim[31] and Venturoli,[32] we partitioned the simulation box into zones, each defined by a range of probe−lipid separation distances. The zones are considered to be "solvation shells" around the probe, each containing an integer number of DPPC lipids at any particular instant. We define the nth solvation shell as an annulus containing $6n$ lipids on average, as specified by the inner and outer radii that satisfy this condition.

A simple way to partition the molecules into shells is to consider only the projections of the molecular centers-of-mass (COM) $\boldsymbol{\rho}$ onto the 2D plane of the bilayer (Figure 2). Taking the reference molecule COM $\boldsymbol{\rho}_R$ as the origin of a 2D coordinate system, the reference−lipid separation distance r is defined as

$$r = \|\boldsymbol{\rho}_R - \boldsymbol{\rho}_L\| \quad (1)$$

where $\boldsymbol{\rho}_L$ is the lipid COM. Positional correlations in fluid phases are short-range, and therefore, the $\boldsymbol{\rho}_L$ are nearly randomly distributed. Under this assumption, shell n has an

dx.doi.org/10.1021/jp400289d | J. Phys. Chem. B 2013, 117, 4844−4852

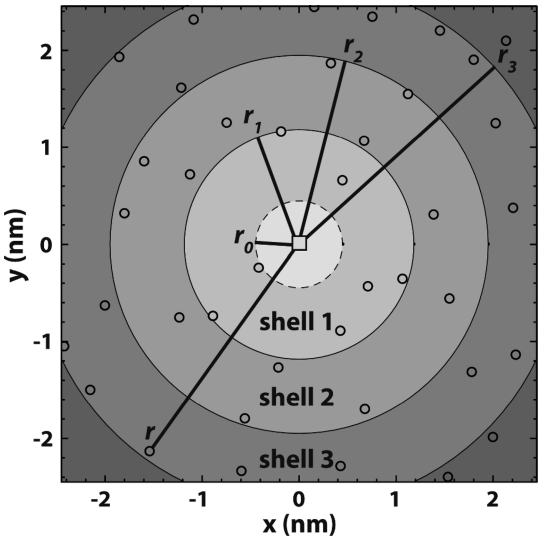

Figure 2. Partitioning of DPPC into solvation shells (shown for the first three shells). Probe and lipid centers of mass (circles) are projected onto the plane of the bilayer. The reference center of mass (square) is taken to be the origin, and shell inner and outer radii are defined such that shell n contains on average $6n$ lipids (see eq 3). A DPPC molecule is considered to be contained in shell n if $r_{n-1} \leq r < r_n$ (with $r < r_0$ assigned to the first shell for same-leaflet lipids and assigned to shell 0 for opposite-leaflet lipids).

average area of $6nA_L$, where A_L is the average area of a host lipid calculated on a per frame basis (i.e., the total bilayer area divided by the number of lipids per leaflet). Assuming a circular lipid area, the average lipid radius is

$$r_0 = \sqrt{A_L/\pi} \tag{2}$$

The annular radii are then defined as

$$r_n = r_0\left(1 + 6\sum_{i=1}^{n} i\right)^{1/2} = r_0\sqrt{1 + 3n(n+1)} \tag{3}$$

At a given instant (i.e., a particular simulation snapshot), a lipid is considered to reside in shell n if $\boldsymbol{\rho}_L$ falls within the inner and outer radii of the shell, that is, if $r_{n-1} \leq r < r_n$ (with $r < r_0$ assigned to the first shell). An identical approach is used to partition lipids in the leaflet opposite the probe, with the modification that lipids with $r < r_0$ are considered to reside in shell 0. With these definitions, lipids residing in shell $n > 0$ (both leaflets) are directly opposite each other in the bilayer, while shell 0 contains the probe and opposing DPPC molecule. The simulation box was divided into shells 0−10 using this scheme, with all remaining lipids considered to be in the 11th shell. For DiI simulations, the reference molecule was in every case the probe itself. For simulations containing only DPPC, the reference DPPC was randomly chosen in each frame (rather than referencing to the inserted DPPC), which allows for better sampling of the system and so produces more accurate results. This method is justified, as the insertion of DPPC did not influence any aspect of the simulation (data not shown).

In addition to neglecting any short-range positional order of the fluid bilayer, our definition of shells neglects the average area of the probe molecule (which will in general be different than that of the host lipid), as well as any distance-dependent perturbations of lipid areas. Though somewhat crude, the method nevertheless partitions the simulation box such that each shell contains an average of $\sim 6n$ lipids (Supporting Information, Table S1). We note however that, while this type of partitioning is often used, it results in a particularly interesting artifact: lipids with larger areas (and greater disorder) are preferentially "squeezed" into higher shell numbers for same-leaflet lipids (Supporting Information, Figure S1). This is likely because the total shell area increases with shell number, with the result that a lipid with a larger area is more likely to be assigned to a higher shell. A similar phenomenon (though with the opposite result) is seen when using a partitioning scheme based on the Voronoi tessellation (data not shown). In this case, lipids with smaller areas (and higher order) are preferentially squeezed into higher shell numbers. This phenomenon is known from theory and has been studied in 3D simulations of water hydration shells.[33] Therefore, regardless of the partitioning scheme, care must be taken to account for such shell-dependent trends. For our partitioning methodology, we report our average shell measurements as a ratio: we divide the shell n average for a DiI-containing bilayer by the corresponding shell n average for the pure DPPC bilayer.

Finally, we note that, for the purposes of calculating error bars, each leaflet is considered to be an independent simulation (i.e., 12 bilayer simulations yield a total of 24 data sets). We performed a cross-correlation analysis of the parameters discussed in the text (i.e., $\langle S_{CD}\rangle$ and P−N vector orientation) to verify complete independence across simulations for the production run (data not shown). Ratios are reported with error bars corresponding to 95% confidence intervals. In all other cases, error bars correspond to one standard deviation.

3. RESULTS

3.1. Systems Equilibrate within the First 10 ns of Production Run. Simulation equilibration is essential to ensure accurate and realistic results. Area per lipid (APL) is one standard way to determine when a membrane simulation is equilibrated and can be used to check if the system is physically sensible.[34] Figure 3A shows APL versus time for a representative production run of a pure DPPC bilayer. The APL for a given snapshot was calculated as the area of the simulation box divided by the number of lipids per leaflet. For the graph shown, the data were smoothed using boxcar averaging over 10 consecutive frames (black curve). The APL is equilibrated after the first 10 ns (dashed gray line), and indeed, the APL over the last 50 ns never drifts far from the average APL of 63.9 ± 0.6 Å^2 (red line) calculated over the same time. This value is in good agreement with the experimentally measured APL of a pure DPPC bilayer of 63.0 Å^2 at 323 K.[35]

To further confirm the complete equilibration within the first 10 ns of the production run, we looked at the transverse positions of various bilayer components over the full production run. Figure 3B shows the locations of the DPPC phosphorus and nitrogen, and the COMs of the DiI-C18:0 chromophore and entire molecule, for a representative simulation. The bilayer COM is located at $z = 0$ nm. The initial thickness and rapid movement of bilayer components toward the bilayer COM is due to the system transitioning from the NVT to NPT ensemble. After 10 ns, the positions do not fluctuate significantly, nor do they drift. Additionally, as described in ref 20, the DiIs are fully buried within the bilayer by 10 ns and remain oriented with their chromophore close to the water. Similar equilibrations were seen in the systems containing DiI-C18:2 and DiI-C12:0 (Supporting Information,

dx.doi.org/10.1021/jp400289d | J. Phys. Chem. B 2013, 117, 4844−4852

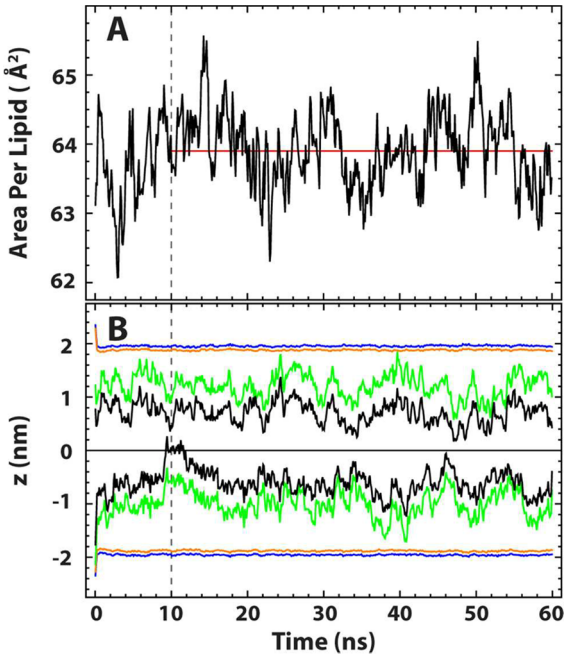

Figure 3. Representative data showing equilibration of simulations within 10 ns. (A) APL during a representative 60 ns simulation of a pure DPPC bilayer. The average value over the final 50 ns (red line) is consistent with the experimentally measured value for DPPC.[34] (B) Transverse bilayer position with respect to the bilayer midplane (z = 0 nm) of DPPC nitrogen (blue) and phosphate (orange) and center-of-mass of the DiI chromophore (green) and entire DiI molecule (black).

Figure S2). These results indicate that the simulations are fully equilibrated within the first 10 ns of the production run, and we therefore use only the last 50 ns for the following analysis.

3.2. DiI Localization. A snapshot of the equilibrated bilayer at the end of a production run is shown in Figure 4,

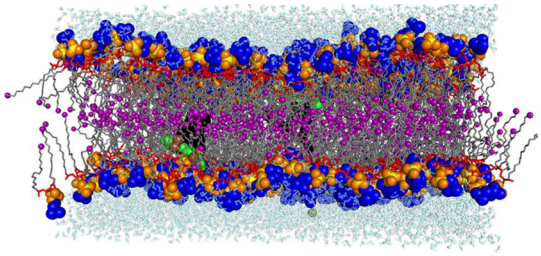

Figure 4. Representative simulation snapshot revealing the DiI-C18:0 location in the bilayer (colors as in Figure 1). DPPC phosphate (orange/yellow) and choline–$(CH_2)_2$ (blue) are shown with space filling spheres, glycerol–carbonyl (red) and methylene groups (gray) are shown as sticks, and terminal methyls (purple) as small spheres. The DiI chromophore (green) is found beneath the DPPC headgroups, predominantly within the hydrophobic interior of the bilayer. Chloride ions (green spheres) were added to neutralize the positive charge of the DiI chromophore. Water (aqua and white) is shown as ball and sticks.

demonstrating the DiI location within the hydrocarbon-dense region of the bilayer. Average mass density profiles shown in Figure 5 further reveal trends for the DiI position within the bilayer, confirming the probe location and orientation with respect to the bilayer interface over the last 50 ns. These data are in agreement with previous simulations.[20] Mass density

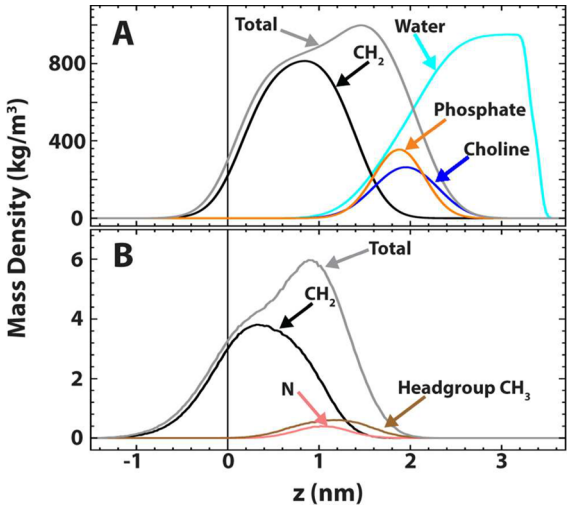

Figure 5. Average single-leaflet mass density profiles. (A) Average densities of DPPC components and water for pure DPPC simulations. (B) Average densities for DiI-C18:0 components reveal its location and orientation within the bilayer. The bilayer midplane is at z = 0 nm.

profiles for DiI-C18:2 and DiI-C12:0 are included in the Supporting Information (Figure S3).

Each simulation consists of two DiI molecules, one in each leaflet. The position of the two probes with respect to each other is an important aspect of our analysis: Since we wish to study the probe's effect on lipids in the same and opposing leaflets, it is important that the two DiI molecules remain well-separated to minimize competing effects on nearby lipids. Using the shell partitioning scheme described in Simulation Methods, we find that the DiI molecules are located ~10 shells apart for most of the simulation, with an average separation distance of 7.4 ± 0.7, 7.1 ± 0.7, and 7.2 ± 0.9 nm (for DiI-C18:0, DiI-C18:2, and DiI-C12:0, respectively). We conclude that probe effects seen in the first few solvation shells are unlikely to be influenced by the opposite-leaflet probe.

3.3. DiI Is Significantly More Disordered than DPPC. To assess the differences between the DiI and DPPC molecules at an atomic level, we measured the order parameter of their hydrocarbon chains. We calculated carbon-deuterium order parameters for lipid chains as

$$S_{CD} = \langle 3\cos^2\theta - 1\rangle/2 \quad (4)$$

where θ is the angle between the C–D bond and the magnetic field (chosen to be parallel to the membrane normal); locations of the deuterium atoms were calculated on the basis of ideal bond geometry.

The average segmental S_{CD} profiles for the reference molecule chains are shown in Figure 6. (N.B. Carbon numbering for a chain starts at the carbonyl carbon for DPPC and at the first methylene carbon for the probes; numbering then increases down the chain.) We find that all DiI chains are more disordered than DPPC chains. The saturated 12:0 and 18:0 chains have similar profiles, whereas the double bonds introduce significant disorder in the 18:2 chains. Both the substantial disorder of the probe chains and the location of the bulky chromophore among the DPPC chains raise the possibility of local perturbations of DPPC molecules.

3.4. DiI Perturbs the Order of Nearby Lipids in the Same and Opposing Leaflets. We examined the effect of an inserted DiI molecule on the overall chain order of successive

dx.doi.org/10.1021/jp400289d | J. Phys. Chem. B 2013, 117, 4844–4852

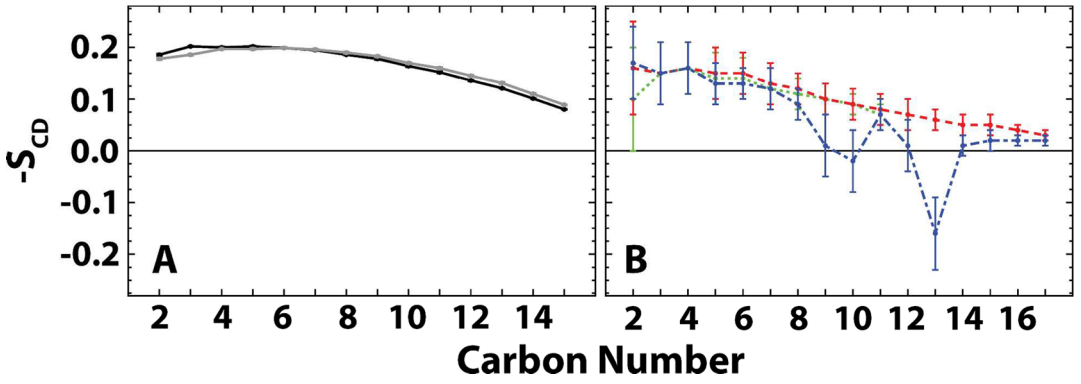

Figure 6. Segmental order parameter profiles for DPPC and DiI probes. (A) DPPC *sn*-1 (black solid) and *sn*-2 (gray solid) profiles from a probe-free bilayer. (B) DiI-C18:0 (red dashed) and DiI-C12:0 (green dotted) show similar order. Double bonds at carbon numbers 9−10 and 12−13 result in significant disordering of the DiI-C18:2 chains (blue dot-dashed). Error bars indicate the standard deviation.

shells of DPPC. The order parameter for each shell was calculated as an average over all DPPC *sn*-1 and *sn*-2 methylene carbons. To quantify the order perturbation induced by the probe, we calculated an order ratio (i.e., the order parameter of a DiI-containing bilayer was divided by the corresponding order parameter of a DPPC bilayer).

Figure 7 shows the distance-dependent order ratio for the three DiI bilayer systems. DiI-C18:0, DiI-C18:2, and DiI-C12:0 (Figure 7A−C, respectively) each perturb same-leaflet lipids to a similar degree, inducing a ∼10−12% *decrease* in chain order in first-shell lipids compared to the pure DPPC bilayer. Interestingly, second-shell lipids show a ∼2−4% *increase* in order. Increased order persists for several shells and then gradually returns toward the unperturbed value.

In the opposite leaflet, DiI-C18:0 and DiI-C18:2 decrease the order of zeroth-shell lipids (i.e., located directly opposite the probe) by ∼9%. Order gradually increases with increasing shell number, exceeds the order of unperturbed DPPC beginning at shell 4, and then gradually decreases toward the unperturbed value. Compared to long-chain DiIs, DiI-C12:0 causes only minor perturbations to zeroth-shell lipids in the opposite leaflet. Beyond the zeroth shell, perturbations are similar for all DiI regardless of chain length: order first increases, followed by a gradual decrease toward the unperturbed state. For all DiIs, the same- and opposite-leaflet order closely match in shells ∼6−9. For shells 10−11, the observed decrease in order is likely due to the effect of the second (opposite-leaflet) DiI. A complete listing of order parameters is included in the Supporting Information (Table S2).

3.5. Carbon Order Perturbation Depends on Shell, Not Carbon Number. To examine dye-induced order perturbations in more detail, we investigated how the segmental order of the DPPC chain varies by shell. Figure 8 shows the DPPC *sn*-1 segmental chain order as a function of shell for shells $n \leq 3$. Distance from the probe is indicated by grayscale dashed lines, with progressively darker gray indicating increasing shell number. The average segmental order profile of a pure DPPC bilayer (solid black line) is shown for comparison.

All three probes perturb the order of nearby, same-leaflet lipids. DiI-C18:0 and DiI-C18:2 also perturb opposite-leaflet lipids, while only minor changes are seen for DiI-C12:0. Despite the differences among the probe chains and between the probe chains and the host DPPC, no carbon appears to be significantly more perturbed than any other. This implies that the magnitude of chain order perturbations occurs uniformly

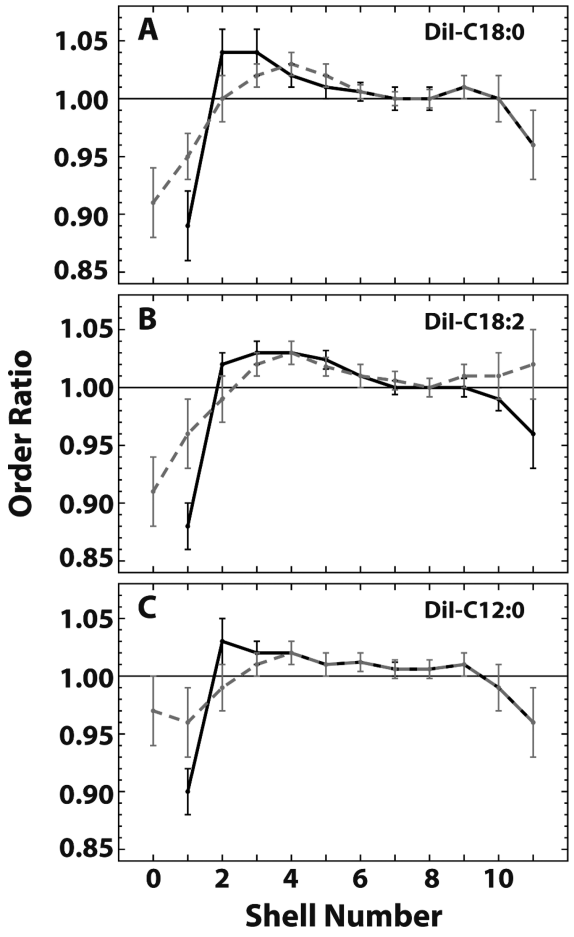

Figure 7. Order ratios reveal DiI-induced perturbations. DPPC order ratio by shell for bilayers containing DiI-C18:0 (A), DiI-C18:2 (B), and DiI-C12:0 (C) for same-leaflet lipids (black solid) and opposite-leaflet lipids (gray dashed). Error bars indicate 95% confidence intervals.

over the length of the DPPC chain, regardless of distance from the probe. These results are similar for the DPPC *sn*-2 chain (Supporting Information, Figure S4).

3.6. DiI Causes Reorientation of Local Lipid Headgroups. We used the same distance-dependent analysis to study the DPPC P−N vector orientation, defined as the angle between the DPPC P−N vector and the bilayer normal [i.e., an angle of 0° (90°) indicates that the P−N vector is

dx.doi.org/10.1021/jp400289d | J. Phys. Chem. B 2013, 117, 4844−4852

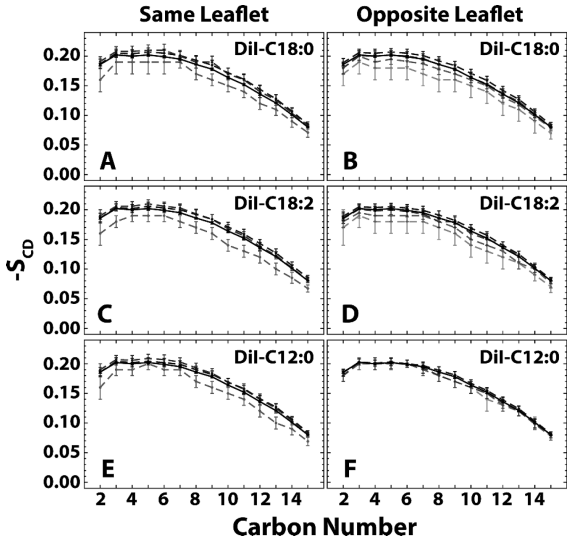

Figure 8. Order perturbations do not vary along chains. Order parameter of DPPC *sn*-1 carbons shown for same-leaflet lipids (left) and opposite-leaflet lipids (right) for bilayers containing DiI-C18:0 (A, B), DiI-C18:2 (C, D), and DiI-C12:0 (E, F). Shells $n \leq 3$ are shown (gray dashed), with darker grays indicating increased shell number. Overall average *sn*-1 order of a pure DPPC bilayer (black solid) is shown for comparison. Error bars indicate the standard deviation.

perpendicular (parallel) to the bilayer plane]. For a pure DPPC bilayer, the average P−N vector orientation was 79.5 ± 0.2°. Figure 9 shows the P−N vector orientation ratio between DiI-

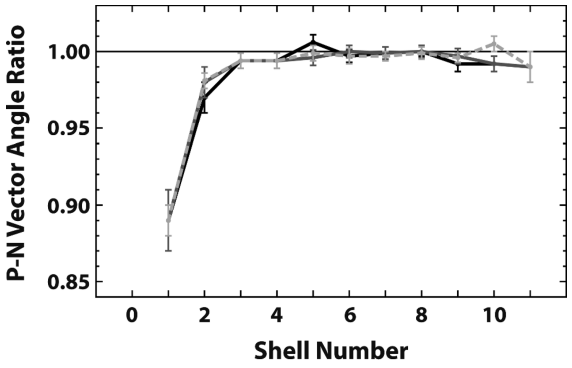

Figure 9. DPPC headgroups preferentially point away from the DiI within the same leaflet. P−N vector angle ratio by shell for same-leaflet lipids in bilayers containing DiI-C18:0 (black), DiI-C18:2 (dark gray), and DiI-C12:0 (light gray dashed), compared to a pure DPPC bilayer. Error bars indicate 95% confidence intervals.

containing and pure DPPC bilayers, for same-leaflet lipids. Compared to a pure DPPC bilayer, the P−N vector of first-shell lipids preferentially points away from the DiI. The P−N angle is ∼11% smaller for shell 1 lipids near a DiI, compared to a pure DPPC bilayer. Significant perturbation also exists in shell 2, before returning to unperturbed values by shell 5. This result indicates that, for DPPC close to a DiI, the P−N vector tends to reorient out of the plane of the bilayer, away from the DiI. In contrast, we did not observe any significant changes in orientation of the P−N vector for opposite-leaflet lipids (Supporting Information, Figure S5). A complete listing of P−N vector angles by shell is included in the Supporting Information (Table S3).

4. DISCUSSION

Perturbations of DPPC by fluorescent probes within the same leaflet are nearly identical for all probes examined. Both acyl chain ordering as well as P−N vector reorientation are similar for same-leaflet DPPC, regardless of the DiI chain length or degree of unsaturation, whereas differences in chain order were observed for DPPC in the opposite leaflet. Looking more closely at why these three different DiI's would have such a similar influence on their nearest neighbor lipids but have different effects on opposite-leaflet lipids, Figure 10 emphasizes

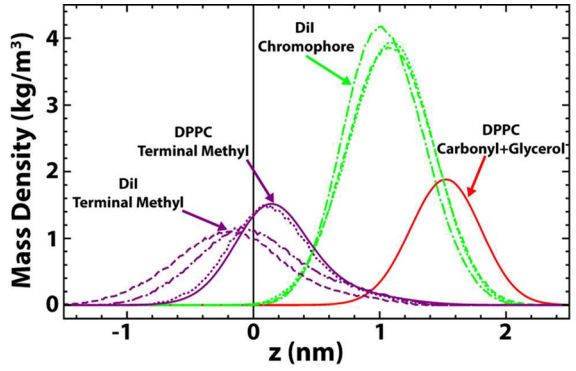

Figure 10. Mass densities show similarities and differences in reference molecule locations. The chromophore (green) of DiI-C18:0 (dashed), DiI-C18:2 (dot-dashed), and DiI-C12:0 (dotted) resides beneath the hydrophilic carbonyl−glycerol group of an average DPPC (red solid). The terminal methyl (purple) of DiI-C18:0 (dashed) and DiIC-18:2 (dot-dashed) shows significant protrusion into the opposing leaflet, whereas DiI-C12:0 (dotted) protrudes to approximately the same extent as an average DPPC (solid). Terminal methyl densities are multiplied by a factor of 4 for visibility, and DPPC densities are reported as an average for a pure DPPC bilayer.

similarities and differences of the DiI. The bulky, positively charged DiI chromophore resides ∼1.0−1.1 nm from the bilayer center, independent of probe chain length or degree of unsaturation. In contrast, the chains themselves, as shown by protrusion of terminal methyls into the opposing leaflet, differ significantly for the three probes. It is reasonable to conclude that these properties are responsible for the observed shell dependent effects.

For the three types of DiI we studied, the positively charged chromophore seems at first glance to be located surprisingly deep in the bilayer. It is likely that the strong delocalization of the charge over a large volume decreases the hydration energy[36,37] and allows for a stable location beneath the lipid headgroups. For a similar chromophore, Krishna and Periasamy found that a variant with two-carbon chains does indeed create a more watery location, but a deep location was also observed,[38] supporting the finding here that the bulky, charged DiI chromophore can be located within the bilayer. Though our simulations are not long enough to predict flip-flop rates, we believe that the chromophore position just beneath the lipid carbonyls is energetically favorable and stable due in part to the bilayer potential. As reviewed by Wang,[39] all-atom membrane simulations show a dipole potential that peaks in the bilayer center. For united atom simulations of a DPPC bilayer, Gullapalli et al. showed that the presence of charged DiI increases the potential difference between the carbonyl region and the bilayer center.[20] Thus, the hydrophobic nature of the

dx.doi.org/10.1021/jp400289d | J. Phys. Chem. B 2013, 117, 4844−4852

DiI drives it into the bilayer, where it is energetically unfavorable for it to flip to the other leaflet.

4.1. Chromophore Location Likely Causes Same-Leaflet Order Perturbations. Despite significant differences in chain length, degree of unsaturation, and order between the DiI molecules tested, the order parameter effects on same-leaflet DPPC were similar for DiI-C18:0, DiIC-18:2, and DiI-C12:0. This implies that the probe chains cannot solely be responsible for the disordering of same-leaflet lipids. This is supported by the observation that all carbons along a DPPC chain are perturbed uniformly and independently of DiI chain structure. Therefore, it is more likely that the bulky headgroup of the DiI and its location within the bilayer have a significant disordering effect on neighboring lipid chains. One possible explanation could be that the DiI chromophore, residing among the hydrocarbon chains, causes the chains to kink. Another possibility is that free space under the DiI chromophore allows for more motional freedom and disordering of the lipids.

The increased order of same-leaflet lipids in shells ∼2−6 reveals that bilayer perturbations do not decay monotonically to the unperturbed state with increasing distance from the probe but instead have a gently oscillating perturbation profile. Damped oscillations in bilayer thickness near protein or lipid inclusions are predicted from theory,[40−42] and arise from an interplay between the perturbing molecule and the mechanical properties of the unperturbed bilayer. The observed behavior may be a manifestation of such mechanical perturbations.

4.2. DiI Charge Changes Local Electrostatic Environment. It was previously observed that, in a 128 lipid system of fluid phase DPPC, the P−N vector angle points out of the bilayer to a greater extent in the presence of charged DiI, whereas no significant change is seen in the presence of uncharged DiI.[20] The authors concluded that the positively charged DiI chromophore was responsible for the DPPC headgroup reorientation, due to electrostatic repulsion. Our results support this conclusion, since we find that DiI has a similar chromophore localization beneath the charged DPPC headgroups, and induces similar DPPC headgroup reorientations, regardless of the probe's alkyl chain structure. Since the nitrogen of the P−N vector and the DiI chromophore are both positively charged, it is likely that electrostatic repulsion is at least in part responsible for the headgroup reorientation out of the bilayer plane and toward the solvent. The gradual decay of P−N reorientation with increasing distance from the chromophore is also consistent with electrostatic repulsion. Furthermore, the decreased order in first-shell lipids increases the area taken up by the hydrophobic chains. We would expect any increased chain area to be accompanied by increased shielding by the hydrophilic headgroup, similar to headgroup shielding of the largely hydrophobic cholesterol according to the umbrella model.[43] However, we observe that, in the presence of DiI, the P−N vector of neighboring DPPC points out of the bilayer to a greater extent, indicating decreased headgroup shielding. This implies that some other effect must be controlling headgroup orientation. We conclude that the location and charge of the chromophore are likely responsible for the observed lipid headgroup reorientations. This would also explain the lack of P−N vector reorientation in opposite-leaflet lipids, as their headgroups are far from the charged chromophore.

4.3. Probe Chain Protrusion Enables Communication of Information across the Bilayer Midplane. DiI can have a significant impact on lipids in the opposite leaflet, as was also seen in MD studies of PyrPC.[16] DiI-C18:0 and DiI-C18:2 caused decreased order in DPPC chains directly across from the probes, whereas DiI-C12:0 did not. We are confident that such effects do not result from the presence of DiI in the opposite leaflet, since the two DiI molecules are separated by ∼7 nm. Rather, this opposite-leaflet effect is likely due to protrusion of the probe hydrocarbon chains into the opposite leaflet. As seen in Figure 10, there is substantial protrusion of DiI chains, which progressively decreases in the series 18:0 > 18:2 > 12:0 ≈ 16:0 (DPPC). This is consistent with the idea that the presence of these chains in the opposite leaflet causes order perturbations, rather than free space beneath the chromophore or other dye properties.

4.4. Small Lipid Domains Are Negligibly Affected by DiI, but Averages Mask Perturbation Trends. When viewed as ensemble averages over all DPPC in a simulation, both acyl chain order and P−N vector orientation show only minimal perturbations. Compared to the ensemble order for a pure DPPC bilayer, changes of 0.6 ± 0.4, 0.6 ± 0.4, and 0.8 ± 0.3% in ensemble order are seen for bilayers containing DiI-C18:0, DiI-C18:2, and DiI-C12:0, respectively. Compared to the ensemble P−N vector orientation in a pure DPPC bilayer, changes of −0.5 ± 0.1, −0.6 ± 0.1, and −0.6 ± 0.1% are seen in ensemble P−N vector orientations for DiI-C18:0, DiI-C18:2, and DiI-C12:0, respectively. Thus, even in a patch of just a few hundred lipids per leaflet, less than a 1% change is seen in both order and P−N vector orientation. We conclude that the probes studied can effectively be used to examine the properties of nanodomains without significant perturbation of average bilayer properties as long as the probe concentrations within the nanodomains remain low.

We caution though that small changes in ensemble averages cannot always be used as a determination of probe fidelity. Some experiments rely on measuring small changes of probe fluorescence properties, and spin-labeled probes in particular report directly on the order of their local environment. Thus, even if these types of probes have a minor effect on ensemble bilayer properties, they could still alter their local order or electrostatic environment and thereby distort measurements. Such significant effects in the same and opposite leaflet would have been masked in these simulations if only average ensemble properties were taken into account. Furthermore, the smaller the simulation size, the greater the extent to which local perturbations near the probe can skew ensemble averages. Obtaining physically relevant and accurate results therefore requires distance-dependent analyses in large simulations which allow enough room for perturbations to both exist and decay. We emphasize that to gain statistically significant results in such systems, when measuring parameters in shells with fewer than 10 lipids, many long simulations are required.

5. CONCLUSIONS

MD simulations are a powerful tool for examining the spatial extent of bilayer perturbations of a fluorescent lipid analogue. Using MD, we find significant perturbations of the local environment of DiI probes, even for lipids across from the probe in the opposite leaflet. For DPPC molecules near a DiI, we observe the following: (1) substantial localized disordering and minor persistent ordering caused by chromophore location and hydrocarbon protrusion and (2) localized headgroup reorientation caused by chromophore location and charge. These small-scale ordering and electrostatic changes are inherently impossible to observe using conventional exper-

imental techniques, especially those which rely on properties of the probe which may themselves be altered by the locally perturbed environment. When analysis is limited to only average bilayer properties, these local probe effects can be misunderstood or even masked altogether. Even though the DiI molecules may significantly perturb local DPPCs, these ensemble averages show that they *do not* significantly alter the properties of nanodomain patches containing a few hundred lipids. Our simulations indicate that at low local concentrations DiI will not alter membrane phase behavior (i.e., phase boundaries and tielines), and can therefore be used reliably to study nanodomains. However, while not a detriment for DiI molecules, the local perturbations caused by fluorescent probe molecules may be critical for other types of probes like spin-labels, which report directly on properties of their local environment. In the future, we plan to investigate other probes to determine if such effects exist, and how large a role they would play in accurately interpreting information reported by the probe.

■ ASSOCIATED CONTENT

Supporting Information

DiI topology files, description of the simulation setup, three tables, and five figures. This material is available free of charge via the Internet at http://pubs.acs.org.

■ AUTHOR INFORMATION

Corresponding Author

*E-mail: gwf3@cornell.edu. Phone: (607) 255-4744.

Notes

The authors declare no competing financial interest.

■ ACKNOWLEDGMENTS

Support was from research awards from the NIH R01 GM077198 and the NSF MCB 0842839 (to G.W.F.). This material is based upon work supported by the National Science Foundation Graduate Research Fellowship under grant number DGE-114153 (to D.G.A.). This work used the Extreme Science and Engineering Discovery Environment (XSEDE), which is supported by National Science Foundation grant number OCI-1053575. A portion of this research was also conducted using the resources of the Cornell Center for Advanced Computing, which receives funding from Cornell University, the National Science Foundation, and other leading public agencies, foundations, and corporations. We thank Alan Grossfield, Jonathan Amazon, Juyang Huang, and Hari Muddana for helpful discussions.

■ REFERENCES

(1) Jahnig, F. *Proc. Natl. Acad. Sci. U.S.A.* **1979**, *76*, 6361−6365.
(2) Klymchenko, A. S.; Mely, Y.; Demchenko, A. P.; Duportail, G. *Biochim. Biophys. Acta* **2004**, *1665*, 6−19.
(3) Sims, P. J.; Waggoner, A. S.; Wang, C. H.; Hoffman, J. F. *Biochemistry* **1974**, *13*, 3315−3330.
(4) Scherfeld, D.; Kahya, N.; Schwille, P. *Biophys. J.* **2003**, *85*, 3758−3768.
(5) Parasassi, T.; De Stasio, G.; Ravagnan, G.; Rusch, R. M.; Gratton, E. *Biophys. J.* **1991**, *60*, 179−189.
(6) Heberle, F. A.; Buboltz, J. T.; Stringer, D.; Feigenson, G. W. *Biochim. Biophys. Acta* **2005**, *1746*, 186−192.
(7) Veatch, S. L.; Keller, S. L. *Biochim. Biophys. Acta* **2005**, *1746*, 172−185.
(8) Bagatolli, L.; Kumar, P. B. S. *Soft Matter* **2009**, *5*, 3234−3248.
(9) Honerkamp-Smith, A. R.; Cicuta, P.; Collins, M. D.; Veatch, S. L.; den Nijs, M.; Schick, M.; Keller, S. L. *Biophys. J.* **2008**, *95*, 236−246.
(10) Heberle, F. A.; Wu, J.; Goh, S. L.; Petruzielo, R. S.; Feigenson, G. W. *Biophys. J.* **2010**, *99*, 3309−3318.
(11) Ethier, M. F.; Wolf, D. E.; Melchior, D. L. *Biochemistry* **1983**, *22*, 1178−1182.
(12) Veatch, S. L.; Leung, S. S.; Hancock, R. E.; Thewalt, J. L. *J. Phys. Chem. B* **2007**, *111*, 502−504.
(13) Lesslauer, W.; Cain, J. E.; Blasie, J. K. *Proc. Natl. Acad. Sci. U.SA.* **1972**, *69*, 1499−1503.
(14) Podo, F.; Blasie, J. K. *Proc. Natl. Acad. Sci. U.S.A.* **1977**, *74*, 1032−1036.
(15) Repakova, J.; Holopainen, J. M.; Morrow, M. R.; McDonald, M. C.; Capkova, P.; Vattulainen, I. *Biophys. J.* **2005**, *88*, 3398−3410.
(16) Repakova, J.; Holopainen, J. M.; Karttunen, M.; Vattulainen, I. *J. Phys. Chem. B* **2006**, *110*, 15403−15410.
(17) Loura, L. M.; Ramalho, J. P. *Biochim. Biophys. Acta* **2007**, *1768*, 467−478.
(18) Loura, L. M.; Fernandes, F.; Fernandes, A. C.; Ramalho, J. P. *Biochim. Biophys. Acta* **2008**, *1778*, 491−501.
(19) Loura, L. M. S.; Ramalho, J. P. P. *Biophys Rev.* **2009**, *1*, 141−148.
(20) Gullapalli, R. R.; Demirel, M. C.; Butler, P. J. *Phys. Chem. Chem. Phys.* **2008**, *10*, 3548−3560.
(21) Hess, B.; Kutzner, C.; van der Spoel, D.; Lindahl, E. *J. Chem. Theory Comput.* **2008**, *4*, 435−447.
(22) Oostenbrink, C.; Villa, A.; Mark, A. E.; van Gunsteren, W. F. *J. Comput. Chem.* **2004**, *25*, 1656−1676.
(23) Berger, O.; Edholm, O.; Jahnig, F. *Biophys. J.* **1997**, *72*, 2002−2013.
(24) Muddana, H. S.; Gullapalli, R. R.; Manias, E.; Butler, P. J. *Phys. Chem. Chem. Phys.* **2011**, *13*, 1368−1378.
(25) Chiu, S. W.; Clark, M.; Balaji, V.; Subramaniam, S.; Scott, H. L.; Jakobsson, E. *Biophys. J.* **1995**, *69*, 1230−1245.
(26) Tieleman, D. P.; Berendsen, H. J. C. *J. Chem. Phys.* **1996**, *105*, 4871−4880.
(27) Van Der Spoel, D.; Lindahl, E.; Hess, B.; Groenhof, G.; Mark, A. E.; Berendsen, H. J. *J. Comput. Chem.* **2005**, *26*, 1701−1718.
(28) Lindahl, E.; Hess, B.; van der Spoel, D. *J. Mol. Model.* **2001**, *7*, 306−317.
(29) Essmann, U.; Perera, L.; Berkowitz, M. L.; Darden, T.; Lee, H. *J. Chem. Phys.* **1995**, *103*, 8577−8593.
(30) Patra, M.; Karttunen, M.; Hyvonen, M. T.; Falck, E.; Lindqvist, P.; Vattulainen, I. *Biophys. J.* **2003**, *84*, 3636−3645.
(31) Kim, T.; Lee, K. I.; Morris, P.; Pastor, R. W.; Andersen, O. S.; Im, W. *Biophys. J.* **2012**, *102*, 1551−1560.
(32) Venturoli, M.; Smit, B.; Sperotto, M. M. *Biophys. J.* **2005**, *88*, 1778−1798.
(33) Voloshin, V. P.; Anikeenko, A. V.; Medvedev, N. N.; Geiger, A.; Stoyan, D. *International Symposium on Voronoi Diagrams in Science and Engineering, 2010*; IEEE Computer Society: 2010; pp 254−259.
(34) Anezo, C.; De Vries, A. H.; Holtje, H.-D.; Tieleman, D. P.; Marrink, S.-J. *J. Phys. Chem. B* **2003**, *107*, 9424−9433.
(35) Kučerka, N.; Nagle, J. F.; Sachs, J. N.; Feller, S. E.; Pencer, J.; Jackson, A.; Katsaras, J. *Biophys. J.* **2008**, *95*, 2356−2367.
(36) Severin, F. F.; Severina, I. I.; Antonenko, Y. N.; Rokitskaya, T. I.; Cherepanov, D. A.; Mokhova, E. N.; Vyssokikh, M. Y.; Pustovidko, A. V; Markova, O. V; Yaguzhinsky, L. S.; Korshunova, G. A.; Sumbatyan, N. V; Skulachev, M. V; Skulachev, V. P. *Proc. Natl. Acad. Sci. U.S.A.* **2010**, *107*, 663−8.
(37) Khuseynov, D.; Fontana, M. T.; Sanov, A. *Chem. Phys. Lett.* **2012**, *550*, 15−18.
(38) Krishna, M. M. G.; Periasamy, N. *Biochim. Biophys. Acta* **1999**, *1461*, 58−68.
(39) Wang, L. *Annu. Rev. Biochem.* **2012**, *81*, 615−35.
(40) Dan, N.; Berman, A.; Pincus, P.; Safran, S. A. *J. Phys. II* **1994**, *4*, 1713−1725.
(41) Pata, V.; Dan, N. *Biophys. J.* **2005**, *88*, 916−924.

(42) West, B.; Brown, F. L.; Schmid, F. *Biophys. J.* **2009**, *96*, 101−115.
(43) Huang, J.; Feigenson, G. W. *Biophys. J.* **1999**, *76*, 2142−2157.